Research Article

Liqing Zhang, Mingqiang Bian, Zhenrong Xiao, Yunyang Wang, Kaicheng Xu*, Baoguo Han, and Hong Huang*

Using nano-$CaCO_3$ and ceramic tile waste to design low-carbon ultra high performance concrete

https://doi.org/10.1515/ntrev-2023-0198
received October 6, 2023; accepted January 10, 2024

Abstract: China's annual production of ceramic tiles inevitably produces a large amount of ceramic tile waste, which causes environmental and land occupation problems. Using a high-volume ceramic tile waste to fabricate ultra high performance concrete (UHPC) will reduce the workability and mechanical properties but increase the low-carbon properties. Motivated by such mechanical and low-carbon properties, this study introduced inexpensive, spherical, low-carbon nano-$CaCO_3$ (NC) to improve the workability and mechanical properties of UHPC with a high volume of ceramic tile waste powder and aggregate (UHPCHCTWPA). The results of this study indicated that NC can improve the workability but shortened the setting times of UHPCHCTWPA. NC also significantly increases the mechanical properties including compressive strength, compressive work, flexural strength, fracture energy, and ratio of flexural strength to compressive strength. It is due to that NC enhances the hydration rate and hydration degree, and optimizes hydration product orientation, size, and distribution. Moreover, compared with UHPC, the UHPCHCTWPA with NC reduces energy intensity, CO_2 emission, and cost by more than 20%. Therefore, adding NC can make UHPCHCTWPA with good workability, mechanical and low-carbon properties and can effectively and quickly utilize ceramic tile waste.

Keywords: ultra high performance concrete, nano-$CaCO_3$, ceramic tile waste, workability, mechanical properties, mechanisms analysis, environmental impact

1 Introduction

In China, there are many ceramic tiles production bases. The ceramic industry has made an important contribution to the development of the economy and society, but it has also resulted in a considerable amount of pollution from ceramic tile waste. At present, most tile wastes are disposed in open stacks or landfills, which easily cause secondary pollution and ecological and environmental problems. Therefore, it is urgent to address ceramic tile waste. As a kind of industrial waste, ceramic tile waste has a high hardness, strength, wear resistance, and oxidation resistance and has the potential to replace natural sand and gravel aggregates. Moreover, the main chemical components of ceramic tile waste are SiO_2 and Al_2O_3. Additionally, finely ground ceramic tile waste powders (CTWPs) have been shown to have some pozzolanic activity and can be used as admixtures [1–8].

Recently, some studies have been done on the workability and mechanical properties of concrete fabricated with ceramic tile waste aggregate (CTWA) as coarse aggregates. Awoyera *et al.* [9] found that the slump of the concrete with CTWA gradually fell from 25 to 100%. Tavakoli *et al.* [10] used CTWA to replace sand when preparing concrete, and the results indicated that when the content of CTWA was 25%, the compressive strength of the concrete increased by 7.85% after curing for 28 days. Alves *et al.* [11] showed that the concrete strength was reduced the most when 50% of the sand was replaced by CTWA, with a compressive strength at 7 day reduced by 24.90% compared to

* **Corresponding author: Kaicheng Xu,** School of Civil Engineering and Architecture, East China Jiaotong University, Nanchang, 330013, China, e-mail: xkcxj@ecjtu.edu.cn
* **Corresponding author: Hong Huang,** School of Civil Engineering and Architecture, East China Jiaotong University, Nanchang, 330013, China, e-mail: Hhong@ecjtu.edu.cn
Liqing Zhang: School of Civil Engineering and Architecture, East China Jiaotong University, Nanchang, 330013, China; Zhongheng Construction Group Co., Ltd, Nanchang, 330200, China; School of Infrastructure Engineering, Nanchang University, Nanchang, 330031, China
Mingqiang Bian, Zhenrong Xiao: School of Civil Engineering and Architecture, East China Jiaotong University, Nanchang, 330013, China
Yunyang Wang: School of Civil Engineering and Architecture, Hunan University of Arts and Science, Changde, 415000, China
Baoguo Han: School of Infrastructure Engineering, Dalian University of Technology, Dalian, 116024, China

the control group. Therefore, Liu *et al.* [12] concluded that the mechanical properties of concrete with CTWA are stronger than those of plain concrete when the CTWA replacement rate does not exceed 40%. In addition, scholars have used CTWPs as admixtures to fabricate green high-performance concrete (HPC) to study its working and mechanical properties. Matos *et al.* [13] showed that the mini slump of HPC with CTWPs progressively fell from 10 to 30%. Sondarva *et al.* [14] used 5% CTWPs to replace cement to fabricate HPC, and found its compressive strength and splitting tensile strength increased by 15.0 and 13.5% at 28 days due to the CTWPs replacement, respectively. Attaelmanan *et al.* [3] and El-Dieb and Kanaan [4] observed similar effects. Mohit and Sharifi [15] found that the compressive strength of HPC at 7 days decreased by 19.83% from 39.88 to 31.97 MPa with the increase in the CTWPs content. In summary, low contents of CTWA and CTWPs can enhance the working and mechanical properties of HPC, but high contents of CTWA and CTWPs may impair the properties. High contents of CTWA and CTWPs can be used to fabricate low-carbon concrete and thus quickly mitigate the ceramic tile waste accumulation problem if their negative effect on the working and mechanical properties can be solved.

Nanomaterials have been introduced into concrete and can improve the properties of concrete. Currently, the commonly used nanomaterials in concrete mainly include carbon nanomaterials, inorganic nonmetallic nanomaterials. and metal oxide nanomaterials [16–19]. Among these nanomaterials, nano-$CaCO_3$ (NC) has the characteristics of low price, spherical shape, low-carbon, and good compatibility with concrete. Moreover, it has been proven that some kinds of NC can improve the working and mechanical properties of concrete. Cui *et al.* [20] studied the workability of sulphoaluminate cement-based reactive powder concrete incorporated with irregular NC, and the results indicated that adding irregular NC reduced the fluidity of reactive powder concrete. Yang *et al.* [21] explored the effect of spherical NC on the workablity of 3D printing concrete and found that the fluidity of 3D printing concrete can be increased by adding the spherical NC. Therefore, the shape of NC is one of the important factors affecting the workability of concrete. Nejad *et al.* [22] concluded that concrete with 0.5% NC had the greatest flexural strength, which has a 45.2% increase compared with the control group. Hakamy [23] found that concrete with 1% NC had the maximum flexural strength and fracture toughness and that its fracture toughness was enhanced by 40.0%. Hodhod and Zaki [24] found that the splitting tensile strength of concrete with 1% NC was highest, with a rise of 80.7%. Sato and Beaudoin [25] found that NC significantly accelerated the hydration of concrete containing large amounts of blast furnace slag and the elastic modulus of concrete with NC was 175.0% higher than that of plain concrete.

Therefore, this study used NC and high content of CTWPs and CTWA (55 and 100%, respectively) to design low-carbon ultra HPC (UHPC), *i.e.*, UHPC with a high volume of ceramic tile waste powder and aggregate (UHPCHCTWPA). UHPCHCTWPA with 0–5% NC was fabricated. Its workability and mechanical properties were investigated. Moreover, the influence mechanisms of NC on UHPCHCTWPA behavior were explored using scanning electron microscopy (SEM), X-ray diffraction (XRD), thermogravimetric (TG), and mercury injection pressure (MIP) analyses. Finally, the sustainability of UHPCHCTWPA with NC was analyzed through material sustainability indicators (MSIs).

2 Materials and test methods

2.1 Materials

The raw materials mainly included cement, CTWPs, CTWA, NC, steel fibers, superplasticizers, and water. The cement used was P·O 52.5, and its chemical composition is shown in Table 1. Moreover, the mean particle size of the cement is 20 μm and its particle size distribution curve is illustrated in Figure 1. The CTWPs were obtained by grinding the ceramic tile waste in a mill for 2 h. The chemical composition of the CTWPs is listed in Table 1. The mean particle size of the CTWPs (as shown in Figure 2(a)) were 10.16 μm and the particle size distribution of the CTWPs is also shown in Figure 1. It can be observed from Figure 1 that the particle size accumulation and particle size density distributions of the CTWPs are similar to those of cement. CTWA with the same chemical composition as CTWPs was used as a fine aggregate with a fineness modulus of 2.02, as shown in Figure 2(b). The NC is spherical (as shown in Figure 3),

Table 1: Main chemical compositions of cement and CTWPs (CTWA)

Chemical composition	Cement (%)	CTWPs (CTWA) (%)
SiO_2	22.35	78.3
Al_2O_3	6.30	15.9
CaO	55.73	0.9
Fe_2O_3	4.91	—
Na_2O	0.07	1.9
K_2O	0.68	2.1
MgO	2.84	0.8
SO_3	2.47	—
R_2O	—	—
Cl^-	—	—
LOI	1.15	—

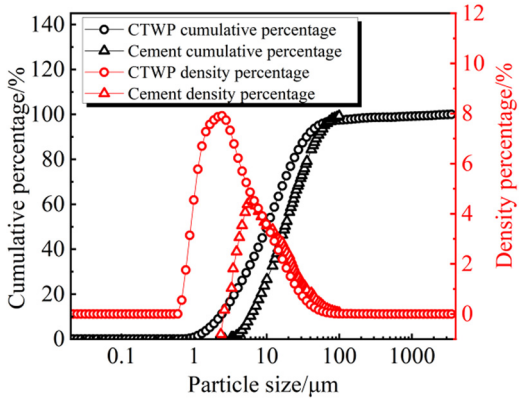

Figure 1: Particle size of cement and CTWPs.

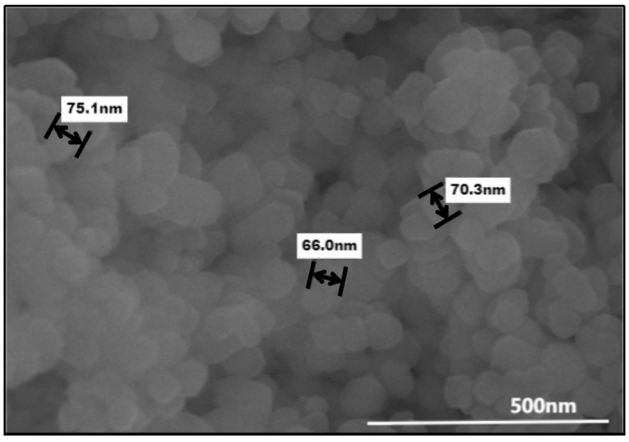

Figure 3: SEM of NC.

and was produced by CO_2 from cement flue gases, with a particle size ranging from 60 to 80 nm. It is white slurry, and its solid content is approximately 71%. The copper-plated steel fibers are flat and straight (diameter is 0.2 mm, length is 13 mm, and tensile strength is ≥2,700 MPa). The solid content of the superplasticizers is 45%, and its water-reducing rate is ≥60%. Additionally, the water used meets the Chinese Concrete Water Standard JGJ63-2006 [26].

2.2 Mix proportions

Table 2 lists the composition of UHPCHCTWPA with NC. The water-to-binder ratio of UHPCHCTWPA was fixed at 0.18. The weight of the CTWPs was 55% of the total binder materials. The copper-plated steel fibers were employed at 2 vol% for all the mixtures. The SP admixture was 2% of the mass of the binder materials. The NC was investigated at 0, 1, 2, 3, 4, and 5% by mass of the binder materials. A total of six groups of UHPCHCTWPA were fabricated by incorporating different NC contents.

2.3 Specimen preparation

Figure 4 shows the preparation method for UHPCHCTWPA with NC. To uniformly disperse the NC, superplasticizers were added to the water as a dispersion agent and mixed with NC, after that, the mixed solution was treated by ultrasonic treatment and high-speed shearing for 10 min. The size of oiled molds is 40 mm × 40 mm × 160 mm. The curing condition of specimens is in tap water at (20 ± 1)°C for 3, 7, and 28 days.

2.4 Test methods

2.4.1 Fresh properties

In this study, the fresh properties of UHPCHCTWPA with NC were characterized by workability and setting times. The fluidity was tested in accordance with GB/T 50080-2016 of China [27], and the setting time tests were conducted according to GB/T 1346-2011 of China [28].

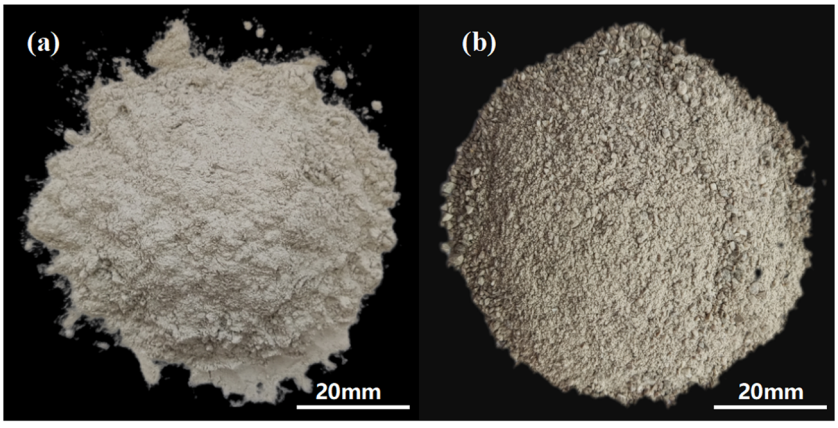

Figure 2: Images of (a) CTWPs and (b) CTWA.

Table 2: UHPCHCTWPA with NC composition

Specimen numbers	Binder materials		CTWA	Water	NC (wt%)	Steel fibers (vol%)	Superplasticizers (wt%)
	Cement	CTWPs					
0% NC	0.45	0.55	1	0.18	0	2	2
1% NC	0.45	0.55	1	0.18	1	2	2
2% NC	0.45	0.55	1	0.18	2	2	2
3% NC	0.45	0.55	1	0.18	3	2	2
4% NC	0.45	0.55	1	0.18	4	2	2
5% NC	0.45	0.55	1	0.18	5	2	2

2.4.2 Mechanical properties

At 3, 7, and 28 days, the mechanical properties of UHPCHCTWPA with NC were tested. The loading rates of the compressive and flexural strengths were 0.1 mm/min and 1.2 mm/min, respectively. The specimen size for three-point bending fracture was also 40 mm × 40 mm × 160 mm and the dimensions of the middle crack are 2 mm in width and 10 mm in height. The loading rate of three-point bending fracture test was 0.1 mm/min. The fracture energy was calculated according to equation (1) [29]. In addition, the method and steps for testing compressive toughness were the same as the compressive strength, and the compressive work was calculated according to equation (2) [30].

$$G_{\mathrm{F}} = \frac{\int_0^{\delta_0} \delta \mathrm{d}\delta}{(h - a_0)t}. \tag{1}$$

where G_{F} is the fracture energy, δ_0 is the value of the deflection at the point of reverse bending in the load–deflection curve, h is the height of the specimen cross-section (m), a_0 is the height of the prefabricated crack (m), and t is the width of the specimen cross-section (m).

$$G_{\mathrm{C}} = \int_0^{\delta_0} \delta \mathrm{d}\delta. \tag{2}$$

where G_{c} is the compressive work, and δ_0 is the value of the deflection at the point of reverse bending in the load–deflection curve.

2.4.3 XRD analysis

The physical phase analysis of the UHPCHCTWPA with NC at 3 and 28 days was performed using an XRD-6100 X-ray diffractometer in the scan range of 10°–90°. The CH crystal orientation was calculated according to equation (3) [31], and the crystallite size of CH was obtained using equation (4).

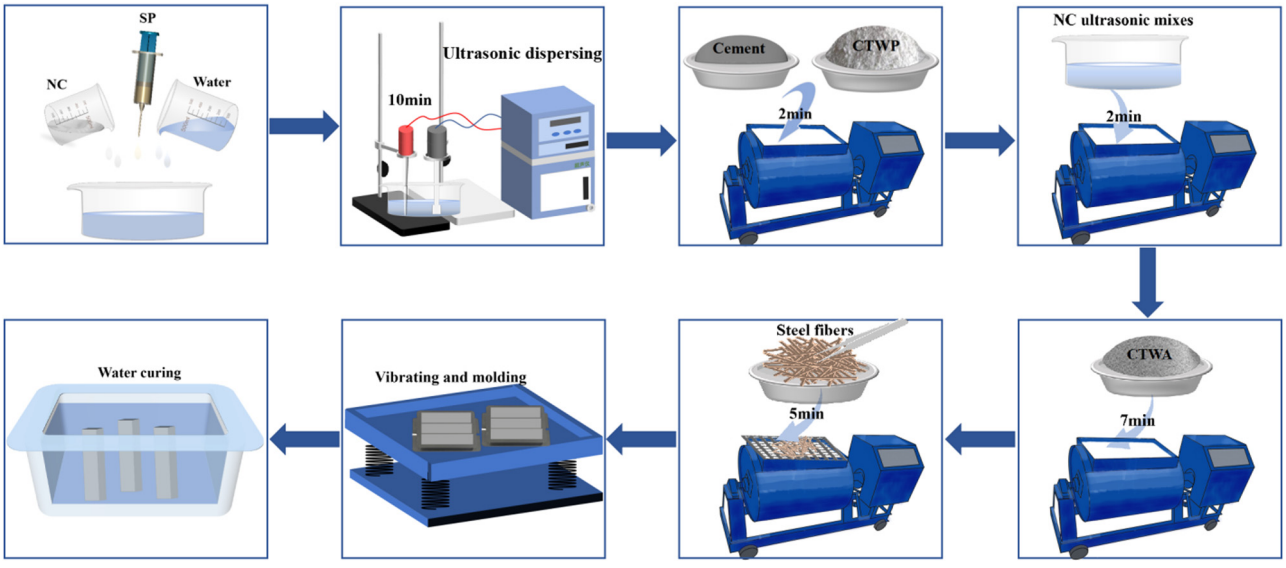

Figure 4: Mixing process of UHPCHCTWPA with NC.

$$I_{CH} = \frac{I_{001}}{I_{101} \times 0.74}, \quad (3)$$

where I_{CH} is the selective orientation degree of CH, and I_{001} and I_{101} are the diffraction peak intensity of the CH at (001) and (101) crystal plane, respectively.

$$D = \frac{K\lambda}{B\cos\theta}, \quad (4)$$

where D is the crystallite size of CH, K is the Scheele's constant and taken as 0.89, λ is the wavelength of X-rays, B is the half-height width of the diffraction peak (rad), and θ is the diffraction angle.

2.4.4 SEM analysis

The interfacial transition zone (ITZ) of UHPCHCTWPA with NC was obtained using a HITACHI SU8010 ESEM at 3 and 28 days. Specimens were cut into small pieces and soaked in anhydrous ethanol for more than 7 days before testing to stop the hydration of the cement.

2.4.5 TG analysis

TG analysis was performed on the UHPCHCTWPA with NC at 3 and 28 days using a Perkin Elmer TGA 4000 TG analyzer. Before the test, the samples were dried at 50°C to a constant weight. The samples were heated from 50 to 1,000°C in nitrogen gas at a heating rate of 10°C/min. The hydration degree of UHPCHCTWPA with NC was calculated by equations (5) [32] and (6) [33].

$$M_{Water} = M_{105} - M_{1000} - M_{CaCO_3}, \quad (5)$$

where M_{Water} is the mass of nonevaporable water (g), M_{105} is the mass of UHPCHCTWPA with NC paste after heat treatment at 105°C for 2 h (g), $M_{1,000}$ is the mass of UHPCHCTWPA with NC paste after heat treatment at 1,000°C for 2 h (g), and M_{CaCO3} is the mass change of UHPCHCTWPA with NC paste caused by the decomposition of $CaCO_3$ during heating (g). Then, the hydration degree of UHPCHCTWPA with NC paste was calculated using equation (6) [33].

$$\beta_t = \frac{M_{Water}}{M_{Water\text{-}Complete}}, \quad (6)$$

where β_t is the 1 g cement hydration degree at hydration time t (%) and $M_{Water\text{-}Complete}$ is the mass of water required for the complete hydration of 1 g cement (g). According to the survey results in the study by Pane and Hansen [33], the $M_{Water\text{-}Complete}$ used in this study was 0.256 g.

2.4.6 MIP analysis

An MIP test using an AutoPore IV 9500 was conducted to evaluate the pore structure of the UHPCHCTWPA with NC at 3 and 28 days. The measurable pore diameter ranged from 3 nm to 800 μm, and the test instrument pressurization ranged from 30 to 60,000 psi (*i.e.*, 0.2–413.7 MPa). In addition, the liquid surface tension σ was taken as 0.485 N/m, and the contact angle θ was taken as 130° to obtain the pore size distribution and total porosity of UHPCHCTWPA with NC.

3 Results and discussion

3.1 Workability and setting time

Figure 5 illustrates the spread-flow value of UHPCHCTWPA with NC. It can be observed from Figure 5 that the spread-flow value of UHPCHCTWPA increased from 545 to 810 mm with the increase in NC content. The regression curves were obtained by linear fitting of the data points, indicating that the spread-flow value increased linearly with the NC content. The spread-flow value of UHPCHCTWPA with 5% NC increased by 48.62% compared to UHPCHCTWPA without NC. NC mainly affects the workability of UHPCHCTWPA through the water absorption effect, ball effect, and replacement effect. Moreover, the ball effect and replacement effect of NC in freshly mixed UHPCHCTWPA were more significant than the water absorption effect. Therefore, NC increased the workability of UHPCHCTWPA [34,35].

Figure 6 presents the setting times of pastes containing NC. As shown in Figure 6, the initial and final setting times decreased as the NC content increased. The initial and final

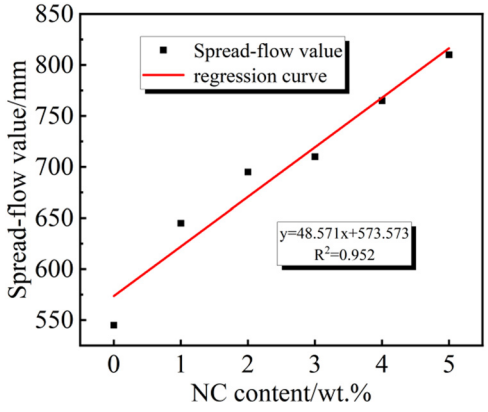

Figure 5: Spread-flow value.

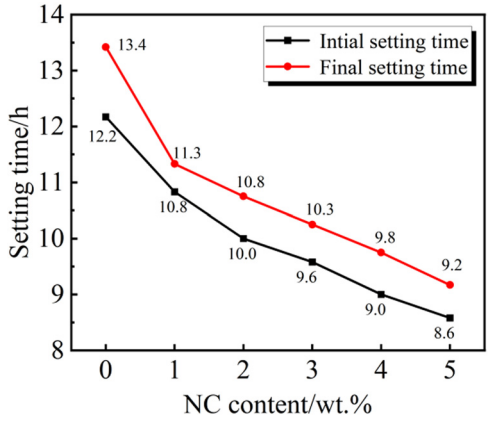

Figure 6: Setting times.

setting times of the UHPCHCTWPA with 5% NC were 8.6 and 9.2 h, respectively, which were 29.5 and 31.7% lower than those of the UHPCHCTWPA without NC. This reduction in setting time did not seem to level off, and the setting time may be further reduced with higher NC content. This may be due to NC having high specific surface area, which can significantly increase in nucleation sites in cement matrix. Due to the nano-core effect, NC can adsorb hydration products and accelerate the hydration of cement and form more hydration products, thus shortening the setting times [34–37].

3.2 Mechanical properties

3.2.1 Compressive strength

The compressive strength of UHPCHCTWPA with various NC contents is shown in Figure 7. Generally, it can be observed from Figure 7 that the compressive strength of UHPCHCTWPA with various NC increases with the increase in curing age. At the same curing age, the compressive strength of UHPCHCTWPA generally showed a parabolic growth tendency with the increase in NC content. When the NC content is 2%, the compressive strength of UHPCHCTWPA was the highest with an increase of 15.2, 14.7, and 17.1% at 3, 7, and 28 days, respectively. With 5% NC content, the compressive strength of UHPCHCTWPA had the lowest rates of increase of 3.6, 7.3, and 6.4% at 3, 7, and 28 days, respectively, but their compressive strengths were still higher than that of UHPCHCTWPA without NC at all curing ages. This indicated that NC has a positive effect on the compressive strength of UHPCHCTWPA.

3.2.2 Compressive deformation and compressive toughness

The compressive load–displacement curves and compressive work of UHPCHCTWPA with various NC are shown in Figure 8. As shown in Figure 8(a), all specimens were in the elastic phase under relatively small compressive loads at 3 days. As the load increased, the rising phase of the load–deformation curve gradually moved toward the *x*-axis, indicating that the UHPCHCTWPA with NC entered the plastic deformation phase. Moreover, NC can increase the peak displacement of UHPCHCTWPA at 3 days. Figure 8(b) presents that the compressive work of UHPCHCTWPA first increased and then decreased as the NC content increased. Compared with UHPCHCTWPA without NC, the compressive work of UHPCHCTWPA with 2 and 3% NC increased by 30.1 and 30.7%, respectively. The compressive load–displacement curves at 28 days are shown in Figure 8(c). As shown in Figure 8(c), the evolution behavior of the

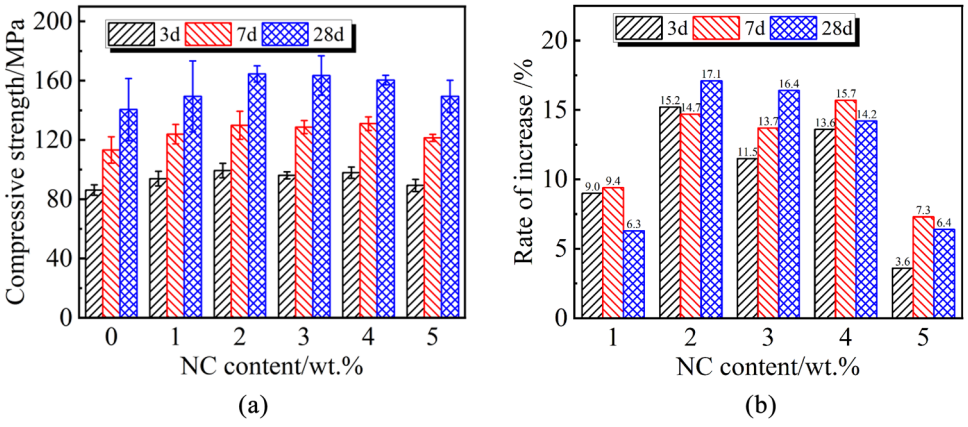

Figure 7: The compressive strength and increase rate of the compressive strength of UHPCHCTWPA with NC. (a) Compressive strength. (b) Rate of increase.

compressive load–displacement curves were similar to that in Figure 8(a). However, the peak load of NC with different dosages is higher than that at 3 days. The compressive work of UHPCHCTWPA with NC at 28 days is shown in Figure 8(d). The compressive work of UHPCHCTWPA with 2% NC was 590.2 J, and its rate of increase was 20.1% compared to UHPCHCTWPA without NC. It can be concluded that NC can effectively enhance the compressive toughness of UHPCHCTWPA and that UHPCHCTWPA with 2% NC had the best toughening effect on UHPCHCTWPA at 3 and 28 days.

3.2.3 Flexural strength

Figure 9 presents the flexural strength and its increase rate of UHPCHCTWPA with NC. As demonstrated in Figure 9, the flexural strengths of UHPCHCTWPA with various NC increased with the increase in the curing age. When the NC content increased, the flexural strength of UHPCHCTWPA first increases and then decreases at the same curing age. Among them, the flexural strength of UHPCHCTWPA with 1% NC was the largest, and the growth rates were 38.5, 29.4, and 34.9 at 3, 7, and 28 days, respectively. Additionally, the increase rate in the flexural strength of UHPCHCTWPA with 2% NC was the smallest, and the corresponding rates of increase were 29.9, 12.6, and 8.2% at 3, 7, and 28 days, respectively, but their flexural strengths were still higher than that of the plain UHPCHCTWPA at all curing ages. Overall, NC had a positive effect on the flexural strength of UHPCHCTWPA especially at the early age.

3.2.4 Flexural deformation and fracture energy

The flexural load–deflection curves and fracture energy of UHPCHCTWPA made with various NC contents are illustrated in Figure 10. Figure 10(a) shows that the load–deflection curves of UHPCHCTWPA with NC exhibit the same variation pattern. The increase in NC content could greatly improve the deflection-hardening behavior of UHPCHCTWPA. Meanwhile, the incorporation of NC increased

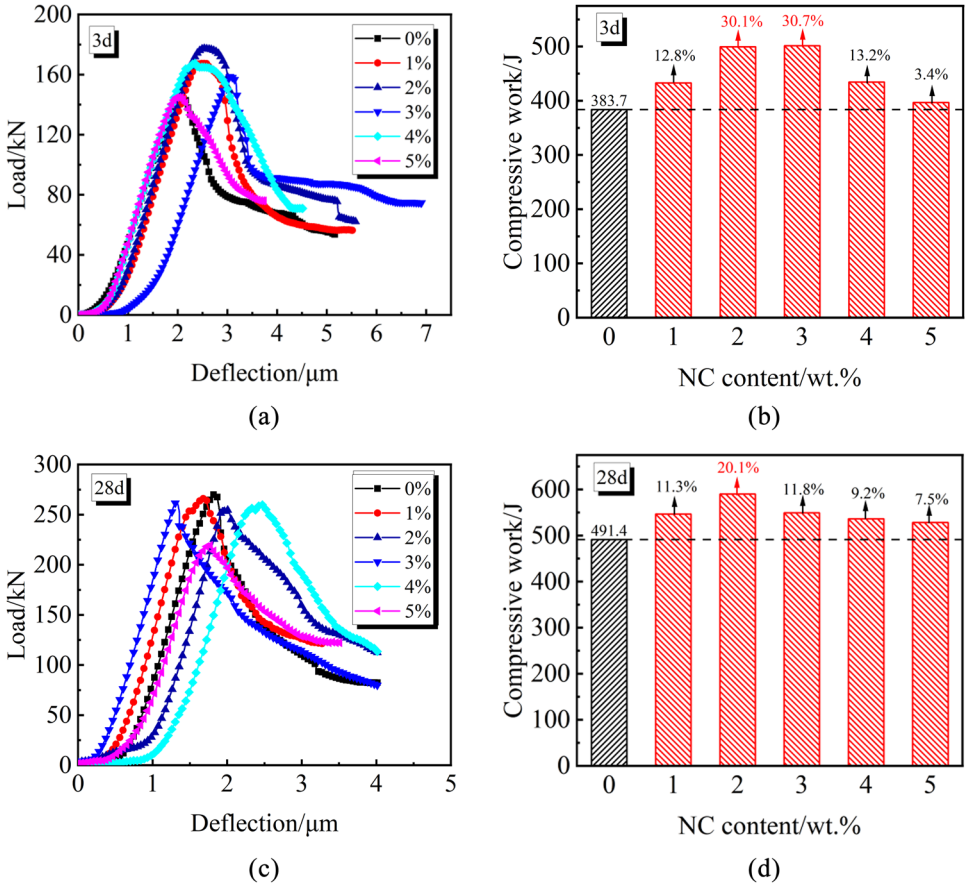

Figure 8: Compressive load–deflection curves and the rate of increase in the compressive work of UHPCHCTWPA with NC. (a) Compressive load–deflection curves at 3 days. (b) Compressive work at 3 days. (c) Compressive load–deflection curves at 28 days. (d) Compressive work at 28 days.

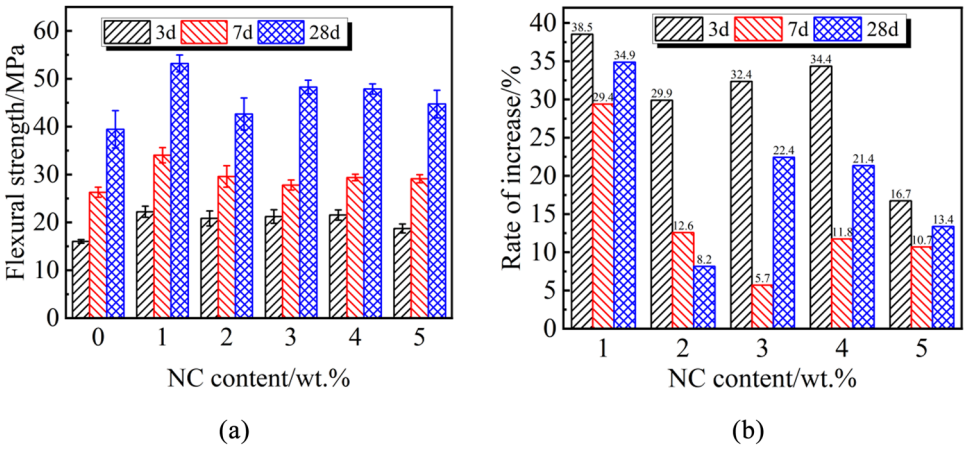

Figure 9: The flexural strength and its increase rate of UHPCHCTWPA with NC. (a) Flexural strength. (b) Rate of increase.

the peak fracture load of the UHPCHCTWPA. This means that NC can improve the fracture behavior of UHPCHCTWPA with NC. According to Figure 10(b), the fracture energy of UHPCHCTWPA showed a parabolic trend with the increase in the NC content. The fracture energies of UHPCHCTWPA with 1, 3, and 4% NC were 6450.1, 6559.7, and 6396.2 J/m^2, respectively. Their rates of increase were 27.5, 29.7, and 26.4, respectively. The flexural load–displacement curves at 28 days are shown in Figure 10(c). As shown in Figure 10(a) and (c), the changing patterns of the flexural load–displacement curves are similar. However, the peak load and ultimate displacement of NC with

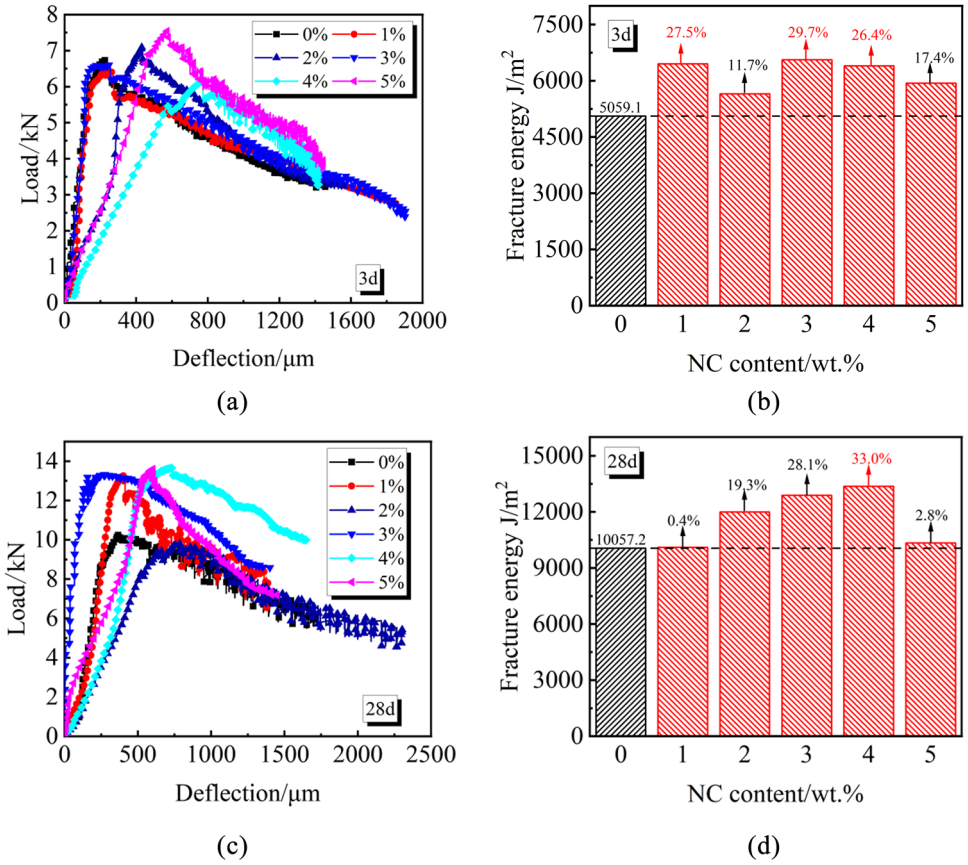

Figure 10: Fracture load–deflection curves and fracture energy of UHPCHCTWPA with NC. (a) Fracture load–deflection curves at 3 days. (b) Fracture energy at 3 days. (c) Fracture load–deflection curves at 28 days. (d) Fracture energy at 28 days.

different dosages were higher than those at 3 days. In Figure 10(d), the fracture energy of UHPCHCTWPA with 4% NC was 13372.5 J/m^2, and its rate of increase was 33.0% compared to UHPCHCTWPA without NC. Therefore, UHPCHCTWPA with NC can withstand higher loads without expanding the microcrack extension [36]. In addition, NC could effectively enhance the flexural toughness of UHPCHCTWPA, and UHPCHCTWPA with 4% NC had the best toughening effect on UHPCHCTWPA at 3 and 28 days.

3.2.5 Flexural strength to compressive strength ratio

Figure 11 presents the flexural strength to compressive strength ratio of UHPCHCTWPA with NC and their rates of increase. It can be observed from Figure 11 that the ratio of flexural strength to compressive strength of UHPCHCTWPA first increased then decreased as the NC content increased. On adding 1% NC, the ratio of flexural strength to compressive strength of UHPCHCTWPA increased by 27.1, 18.2, and 26.9% at 3, 7, and 28 days, respectively. With 2% NC, this ratio increased by 12.8% at 3 days and decreased at 7 and 28 days, but the decreases were insignificant. Therefore, it could be concluded that a suitable content of NC can improve the ratio of flexural strength to compressive strength of UHPCHCTWPA, thus enhancing its flexibility.

3.3 Mechanistic analysis

3.3.1 XRD analysis

The XRD patterns were used to investigate the effect of NC on the physical phase characteristics of the hydration products of UHPCHCTWPA. Figure 12 presents the XRD patterns of UHPCHCTWPA with 0, 1, and 4% NC after curing for 3 and 28 days. As shown in Figure 12, the incorporation of NC did not affect the type of hydration products of UHPCHCTWPA. However, it can be observed from Figure 13 that adding NC can decrease the crystal orientation of the CH, where the crystal orientation of the CH could significantly reduce the crystal orientation of UHPCHCTWPA with 1% NC at 3 days by 40.8%. Moreover, as per the crystallite size of CH shown in Figure 14, it can be found that the crystallite size of the CH in the UHPCHCTWPA with NC was smaller than that in the plain UHPCHCTWPA. The crystallite size of CH in UHPCHCTWPA with 4% NC was 251 Å, which was 27.7% lower than that in UHPCHCTWPA without NC at 3 days. Figure 13 also shows that the crystallite size of the CH in the UHPCHCTWPA with 1% NC was 261 Å at 28 days, which was 28.7% lower than the crystallite size of the CH in the UHPCHCTWPA without NC. In other words, the incorporation of NC decreased the crystal orientation and crystallite size of the CH. This result indicated that the structure of UHPCHCTWPA with NC is very dense and has excellent mechanical properties on a macroscopic scale.

3.3.2 SEM analysis

Figure 15 presents SEM images of the ITZs of UHPCHCTWPA with 0, 1, and 4% NC at 3 and 28 days. In addition, Image J software was used to segment the SEM images with bars, and the width of the ITZ was characterized by the average grayscale value of the bars as shown in Figure 16. It can be observed from Figure 16 that the ITZ width gradually became narrower with the greater incorporation of

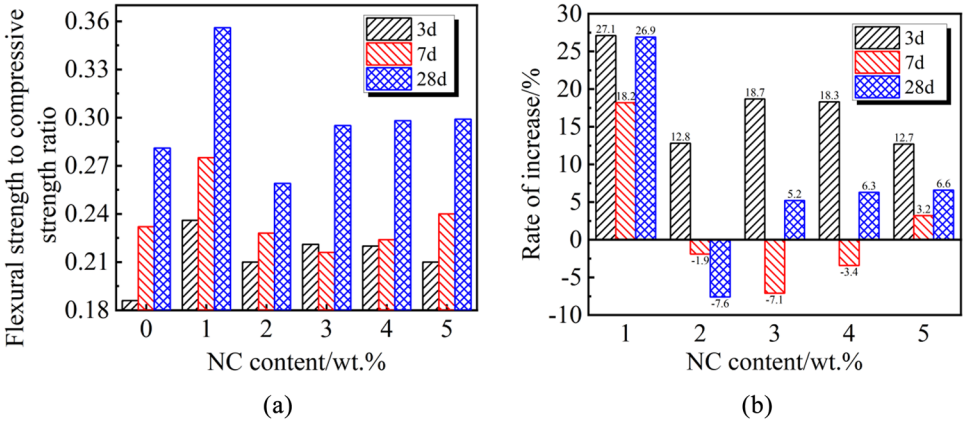

Figure 11: The ratio of flexural strength to compressive strength and its increase rate of UHPCHCTWPA with NC. (a) Flexural strength to compressive strength ratio. (b) Rate of increase.

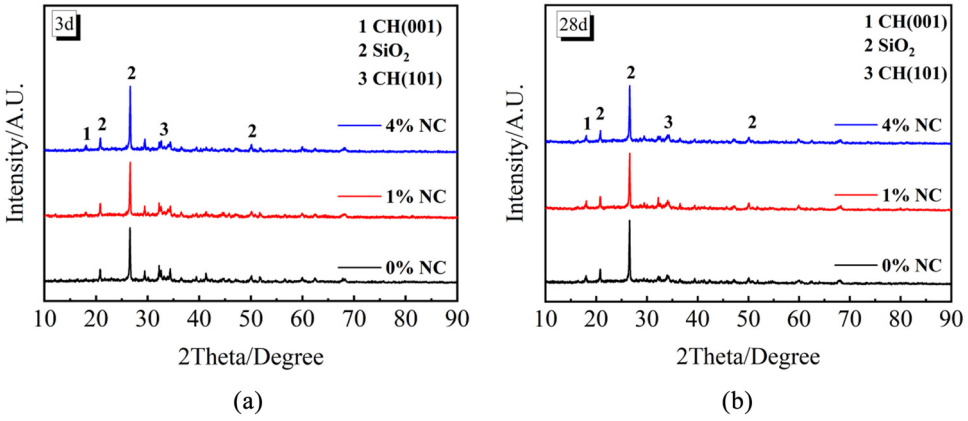

Figure 12: XRD patterns. (a) At 3 days. (b) At 28 days.

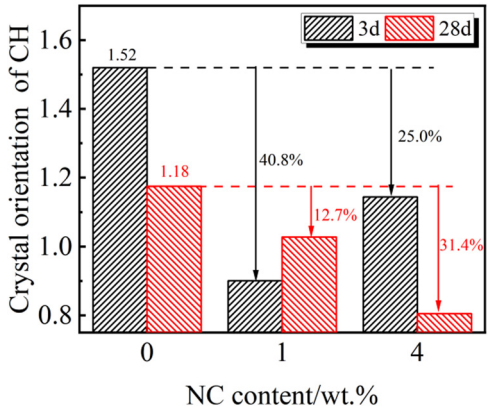

Figure 13: Crystal orientation of CH.

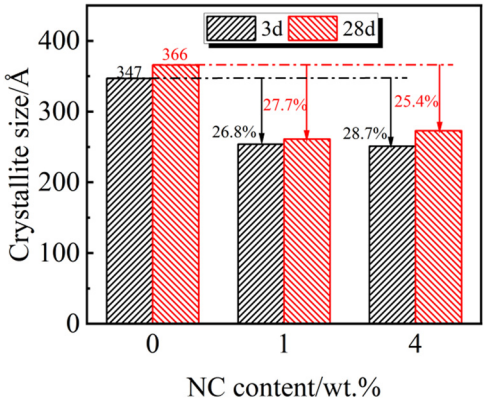

Figure 14: Crystallite size of CH.

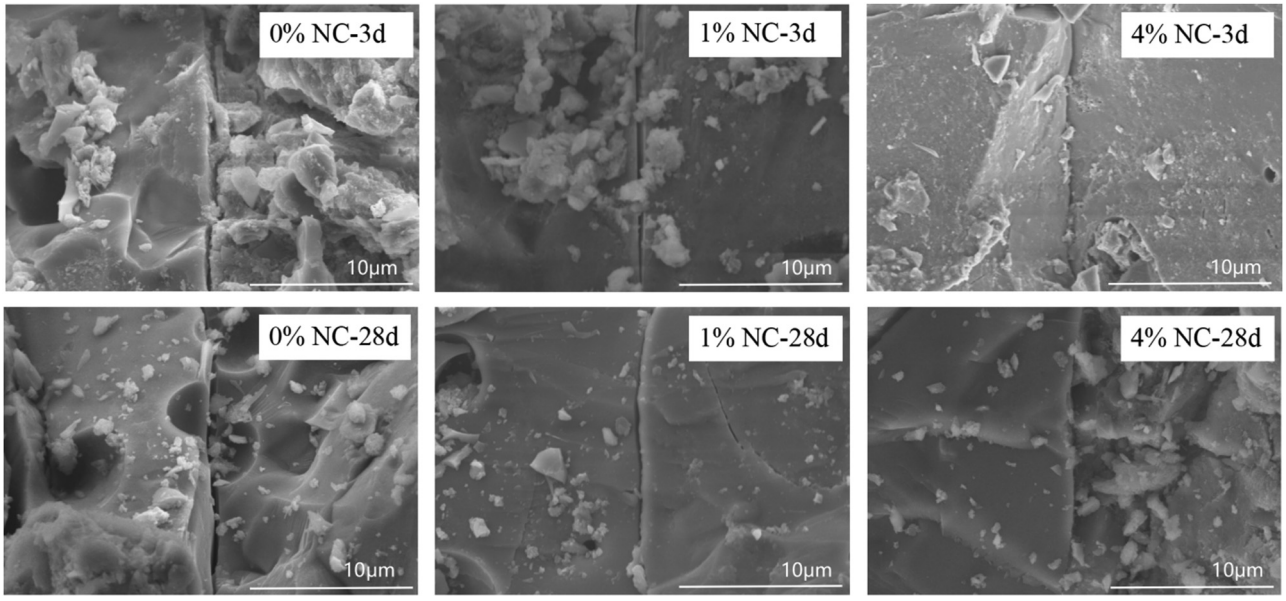

Figure 15: SEM images of ITZs.

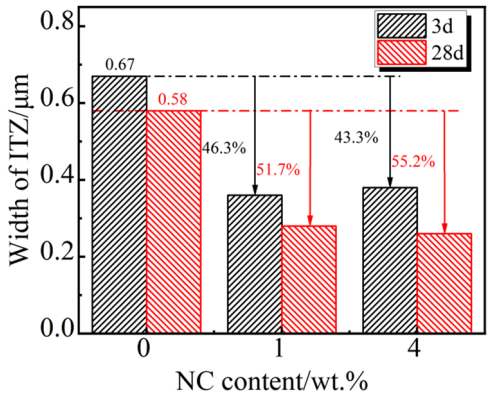

Figure 16: ITZ widths.

NC and longer curing age. Compared to those of UHPCHCTWPA without NC at 3 and 28 days, the ITZ widths of the UHPCHCTWPA with 4% NC were reduced by 46.3 and 55.2%, respectively. Due to the high surface energy, NC can absorb hydration products and finally formed a large number of nanocore-shell elements. Therefore, the pores between the aggregate and slurry filled, making the matrix structure much denser [37–39]. Therefore, NC optimized the ITZs of UHPCHCTWPA and improved its mechanical properties.

3.3.3 TG analysis

Figure 17 presents the TG/DTG analysis curves of UHPCHCTWPA with 0, 1, and 4% NC at 3 and 28 days. Additionally, the hydration degree of the UHPCHCTWPA with NC was calculated based on the TG/DTG analysis curves, as shown in Figure 18. It was clearly noted from Figure 18 that the hydration degree of UHPCHCTWPA can be significantly enhanced by using NC. The hydration degrees of the UHPCHCTWPA with 1 and 4% NC increased by 60.8 and 87.0% at 3 days, respectively. However, the incorporation of NC had little influence on the hydration degree at 28 days, and the fluctuation range was within ±6%. Therefore, the early mechanical properties of UHPCHCTWPA may be enhanced mainly due to the effect of NC on the degree of hydration [24,38,40,41].

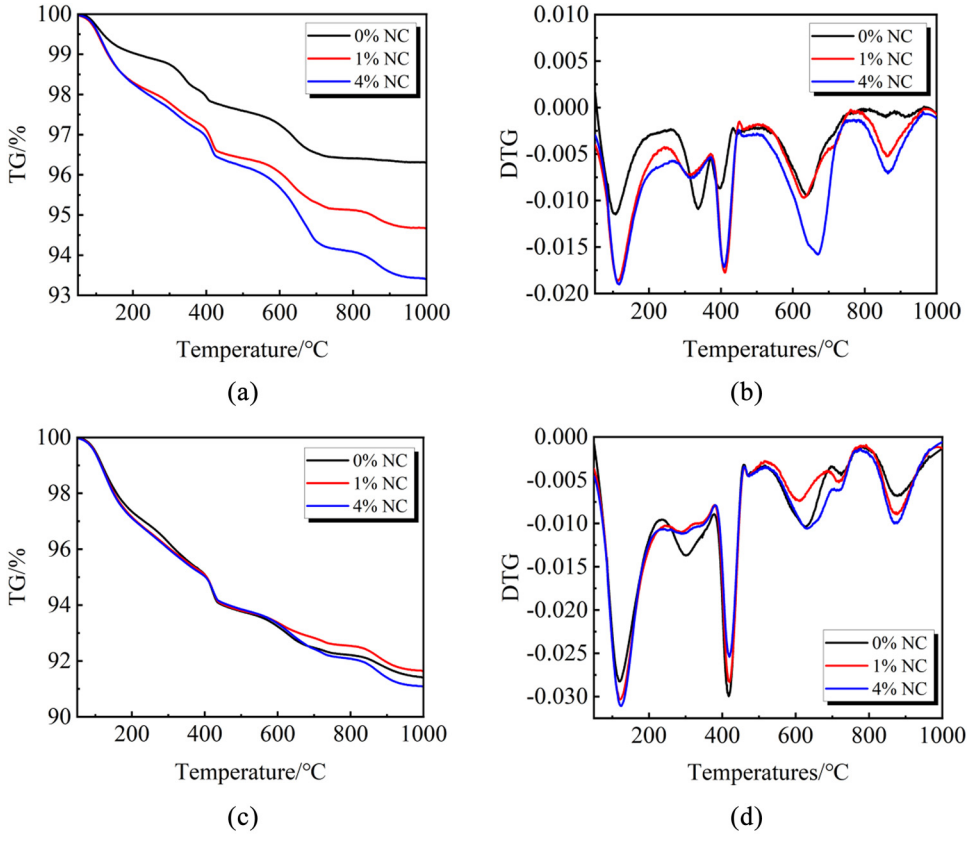

Figure 17: TG/DTG diagram at 3 and 28 days. (a) TG diagram at 3 days. (b) DTG diagram at 28 days. (c) TG diagram at 28 days. (d) DTG diagram at 28 days.

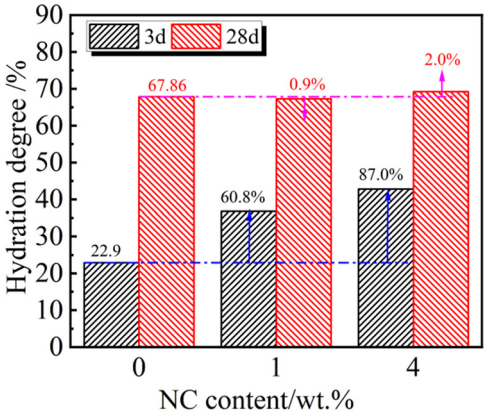

Figure 18: Hydration degree.

3.3.4 MIP analysis

Figures 19 and 20 present the differential cumulative pore size distribution curves and pore size distribution curves of the UHPCHCTWPA with 0, 1, and 4% NC at 3 and 28 days, respectively. It can be seen from Figures 19 and 20 that the most available pore sizes of UHPCHCTWPA were mainly concentrated in the range of 10–100 nm. The peak value of most available pore sizes for UHPCHCTWPA with 4% NC is higher than that of UHPCHCTWPA without NC at 7 days, but the most available pore sizes for UHPCHCTWPA with 4% NC is smaller than that of UHPCHCTWPA without NC at 28 days. Moreover, the peak value greater than 10,000 nm for UHPCHCTWPA with NC is lower than that of UHPCHCTWPA without NC at 7 and 28 days. Figure 21 shows the specific volume proportion of different pores of the UHPCHCTWPA with 0, 1, and 4% NC. As shown in Figure 21, the percentage of the <20 nm pore volume increased from 17.07 to 24.88% and the percentage of the >200 nm pore volume decreased from 64.53 to 37.78% in the UHPCHCTWPA with 4% NC at 3 days compared with the plain UHPCHCTWPA. Moreover, the percentage of the <20 nm pore volume increased from 15.07 to 68.43%, and the percentage

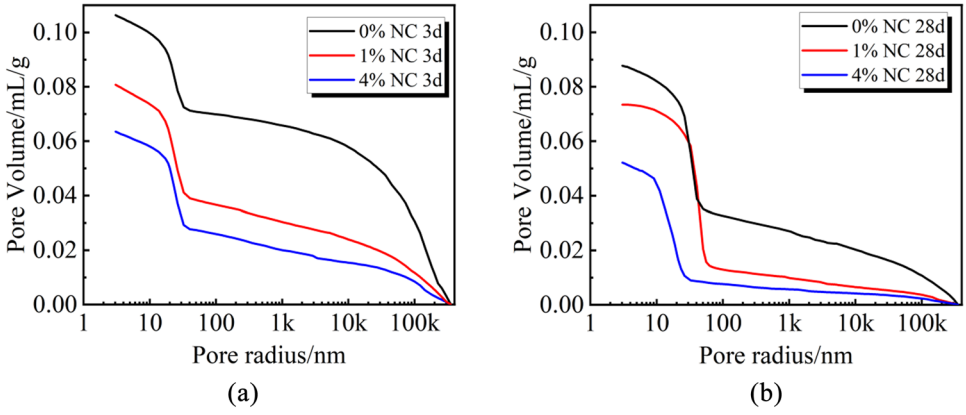

Figure 19: Cumulative pore size distribution curve. (a) At 3 days. (b) At 28 days.

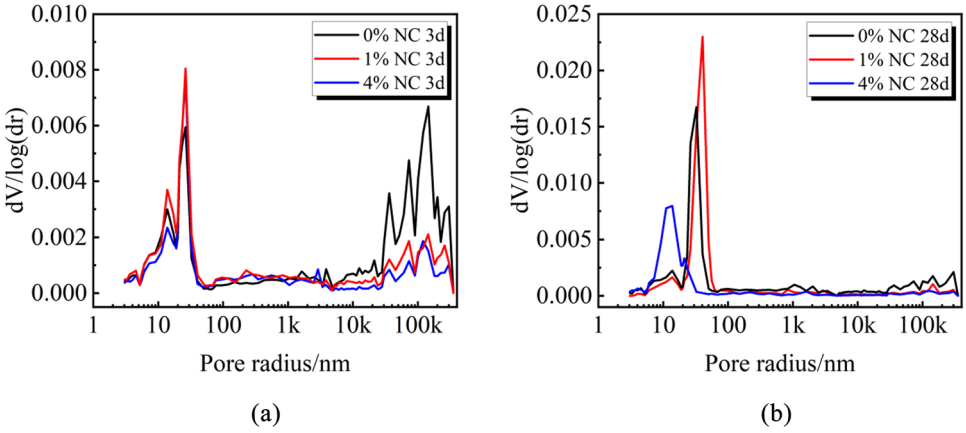

Figure 20: Differential pore size distribution curve. (a) At 3 days. (b) At 28 days.

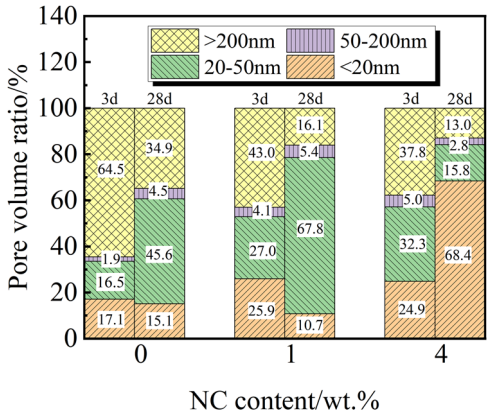

Figure 21: Pore volume ratio.

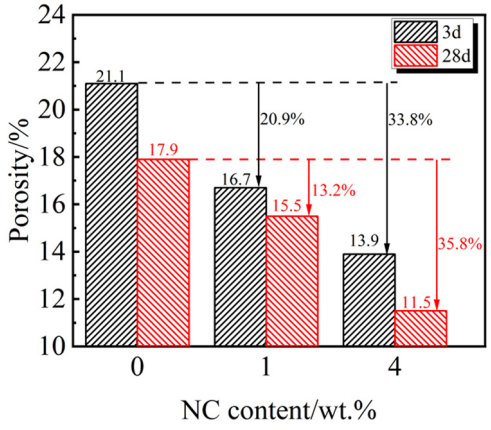

Figure 22: Porosity.

of the >200 nm pore volume decreased from 34.87 to 13.03% in the UHPCHCTWPA with 4% NC at 28 days compared to the UHPCHCTWPA without NC. Therefore, NC could reduce large micropores and increase small micropores of UHPCHCTWPA. Figure 22 shows the porosity of UHPCHCTWPA with 0, 1, and 4% NC. Figure 22 shows that the porosity was 13.98 and 11.46% for the UHPCHCTWPA with 4% NC at 3 and 28 days, which was reduced by 33.8 and 35.8% compared to the UHPCHCTWPA without NC, respectively. NC can optimize the porosity size and effectively reduce the porosity of UHPCHCTWPA due to the nano-core effect [42], which makes UHPCHCTWPA more uniform and denser and improves the mechanical properties.

Table 3: MSIs and cost data of raw materials

Materials	Energy intensity (MJ/kg)	CO_2 emission (kg/kg)	Cost (RMB/ton)
Cement	5.5	0.96	680
Silica sand	0.081	0.0048	600
Silica fume	0.1	0.008	900
CTWP	1.4	0.37	360
CTWA	0.006	0.0015	200
Water	0.001	0.00	2
NC	25.56	-32.04	870
Steel fibers	17.68	2.20	10,000
SP	0.30	0.028	10,000

3.4 Environmental impact and cost analysis

The study uses the MSIs method to quantitatively evaluate the environmental impact of UHPCHCTWPA with NC. The MSIs are determined based on the material and energy flow in the manufacturing process, and are represented by the energy intensity and CO_2 emissions [43,44].

Table 3 lists the energy consumption, CO_2 emission, and unit price of the raw materials. The energy and CO_2 emission of CTWPs and CTWA were calculated during their processing, and the price included the cost of laboratory processing and the cost of recycled materials. In addition, the production of NC can absorb CO_2 from cement flue gases and the production of NC. According to the research of Batuecas *et al.* [45], producing 1 kg of material consists of 98% Portland cement and 2% NC produces 0.3 kg CO_2 whereas producing 1 kg of Portland cement produces 0.96 kg CO_2. It can be calculated that 1 kg of NC produced by this technology can reduce CO_2 emission by 32.04 kg. Therefore, the carbon intensity of NC is negative. Table 4 presents the

Table 4: MSIs and cost comparison of UHPC and UHPCHCTWPA with NC

Type of concrete	Energy intensity (MJ/m^3)	CO_2 emission (kg/m^3)	Cost (RMB/ton)
UHPC (90% cement + 100% silica sand + 10% silica fume + steel fibers + water + SP)	8505.71	1333.65	3067.08
UHPCHCTWPA with 1% NC	6480.67	1032.91	2386.99
UHPCHCTWPA with 2% NC	6507.63	996.38	2388.21
UHPCHCTWPA with 3% NC	6524.59	959.85	2389.42
UHPCHCTWPA with 4% NC	6541.55	923.32	2390.64
UHPCHCTWPA with 5% NC	6558.51	886.79	2391.86

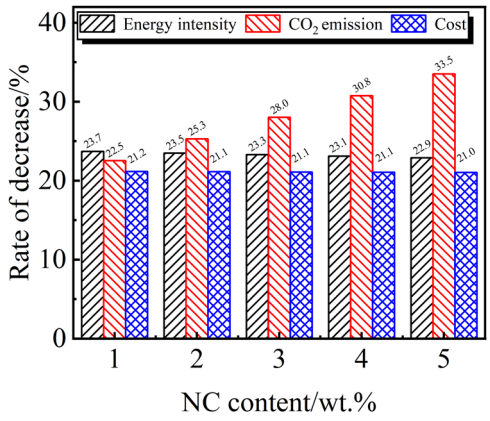

Figure 23: The rate of decrease in the energy intensity, CO_2 emission, and cost of UHPCHCTWPA with NC compared with HPC.

MSIs and cost comparison of UHPC and UHPCHCTWPA with NC. It can be observed from Table 4 that the energy intensity and cost of UHPCHCTWPA increase gradually as the NC content increases but it is still lower than UHPC. Moreover, it is worth noting that the CO_2 emission decreases gradually when the NC content increases. As shown in Figure 23, compared with UHPC, the UHPCHCTWPA with NC reduces energy intensity and cost by more than 20%. Combined with the mechanical properties in this study, UHPCHCTWPA with 1 and 4% NC are relatively optimal. The CO_2 emission of UHPCHCTWPA with 1 and 4% NC is reduced by 22.5 and 30.8% respectively compared with UHPC. Therefore, UHPCHCTWPA with NC is green and sustainable. If applied to industrial production rather than laboratory production, the MSIs and cost will be further reduced.

4 Conclusion

In this study, the effect of NC on the workability and mechanical properties of UHPCHCTWPA was explored in terms of its spread-flow value, setting time, flexural strength, fracture toughness, compressive strength, compressive toughness, and ratio of flexural strength to compressive strength. The mechanisms of NC on the mechanical properties of UHPCHCTWPA was elaborated by XRD, SEM, TG, and MIP analyses. Finally, the sustainability of UHPCHCTWPA with NC was analyzed through MSIs and cost, and findings obtained from this study are as follows.

1) The UHPCHCTWPA with NC increased the workability by 48.62% but shortened the initial and final setting times by 29.5 and 31.7%, respectively.
2) The incorporation of NC was effective in improving mechanical properties of UHPCHCTWPA. The compressive strength, compressive work, flexural strength, fracture energy, and ratio of flexural strength to compressive strength increased by 17.1, 30.7, 38.5, 33.0, and 27.1%, respectively.
3) NC can accelerate the hydration rate and increase the hydration degree by 87% and reduce the selective orientation of CH by 40.8%, the crystallite size of CH by 28.7%, the ITZ width by 55.2%, and the porosity by 35.80%. Thus, the incorporation of NC can enhance the mechanical properties of UHPCHCTWPA.
4) By adding CTWPs, CTWA, and low-carbon NC, the environmental impacts and cost of UHPC can be significantly reduced. Compared with UHPC, the energy intensity and cost of UHPCHCTWPA with NC were both reduced by more than 20%. Even CO_2 emission had fallen by more than 30%.

Funding information: This study was funded by the National Natural Science Foundation of China (52368031 and 52368016), China Postdoctoral Science Foundation (2022M713497), Natural Science Foundation of Jiangxi Province (20224BAB204067), State Key Laboratory of Performance Monitoring and Protecting of Rail Transit Infrastructure, East China Jiaotong University (HJGZ2022201).

Author contributions: Liqing Zhang: investigation, data curation, writing – review and editing, and funding support; Mingqiang Bian: investigation, data curation, writing – original draft, and writing – review and editing; Zhenrong Xiao: data curation and writing – original draft; Yunyang Wang: methodology, validation, and writing –review; Kaicheng Xu: methodology, supervision, and funding support; Baoguo Han: writing – review, methodology, and validation; Hong Huang: supervision and funding support. All authors have accepted responsibility for the entire content of this manuscript and approved its submission.

Conflict of interest: The authors state no conflict of interest.

Data availability statement: All data generated or analysed during this study are included in this published article.

References

[1] Subaşı S, Öztürk H, Emiroğlu M. Utilizing of waste ceramic powders as filler material in self-consolidating concrete. Constr Build Mater. 2017;149:567–74.
[2] Li L, Liu W, You Q, Chen M, Zeng Q. Waste ceramic powder as a pozzolanic supplementary filler of cement for developing sustainable building materials. J Clean Prod. 2020;259:120853.
[3] Attaelmanan M, Kambal MEM, Mansour MI. Study the effect of using ceramic waste powder as partial replacement for cement on concrete properties. J Karary Univ Eng Sci. 2021;1(1):1–7.

[4] El-Dieb AS, Kanaan DM. Ceramic waste powder an alternative cement replacement – Characterization and evaluation. Sustain Mater Technol. 2018;17:e63.
[5] Huseien GF, Sam ARM, Shah KW, Asaad MA, Tahir MM, Mirza J. Properties of ceramic tile waste based alkali-activated mortars incorporating GBFS and fly ash. Constr Build Mater. 2019;214:355–68.
[6] Zhang LQ, Shen H, Xu KC, Huang WY, Wang YY, Chen MC, et al. Effect of ceramic waste tile as a fine aggregate on the mechanical properties of low-carbon ultrahigh performance concrete. Constr Build Mater. 2023;370:130595.
[7] Xu KC, Huang WY, Zhang LQ, Fu SC, Chen MC, Ding SQ, et al. Mechanical properties of low-carbon ultra high performance concrete with ceramic tile waste powder. Constr Build Mater. 2021;287:123036.
[8] Zhang LQ, Pan YN, Xu KC, Bi LP, Chen MC, Han BG. Corrosion behavior of concrete fabricated with lithium slag as corrosion inhibitor under simulated acid rain corrosion action. J Clean Prod. 2022;377:134300.
[9] Awoyera PO, Ndambuki JM, Akinmusuru JO, Omole DO. Characterization of ceramic waste aggregate concrete. HBRC J. 2018;14(3):282–7.
[10] Tavakoli D, Heidari A, Karimian M. Properties of concretes produced with waste ceramic tile aggregate. Asian J Civ Eng. 2013;14(3):369–82.
[11] Alves AV, Vieira TF, De Brito J, Correia JR. Mechanical properties of structural concrete with fine recycled ceramic aggregates. Constr Build Mater. 2014;64:103–13.
[12] Liu FL, Liu JH, Ma BG, Huang J, Li HN. Basic properties of concrete incorporating recycled ceramic aggregate and ultra-fine sand. J Wuhan Univ Technol Mater Sci Ed. 2015;30(2):352–60.
[13] Matos P, Sakata RD, Onghero L, Uliano VG, Gleize P. Utilization of ceramic tile demolition waste as supplementary cementitious material: An early-age investigation. J Bulid Eng. 2021;38:102187.
[14] Sondarva PR, Pitroda JR, Gujar R, Soni J. An Experimental investigation on the strength properties of ceramic tiles waste powder based bacterial concrete. Mater Today: Proc. 2022;62:7062–7.
[15] Mohit M, Sharifi Y. Ceramic waste powder as alternative mortar-based cementitious material. ACI Mater J. 2019;116(6):107–16.
[16] Wang YY, Zhang LQ. Development of self-sensing cementitious composite incorporating hybrid graphene nanoplates and carbon nanotubes for structural health monitoring. Sens Actuators A Phys. 2022;336:113367.
[17] Ding SQ, Xiang Y, Ni YQ, Thakur VK, Wang XY, Han BG, et al. In-situ synthesizing carbon nanotubes on cement to develop self-sensing cementitious composites for smart high-speed rail infrastructures. Nano Today. 2022;43:101438.
[18] Ding SQ, Wang XY, Qiu LS, Ni YQ, Dong XF, Cui YB, et al. Self-sensing cementitious composites with hierarchical carbon fiber-carbon nanotube composite fillers for crack development monitoring of a maglev girder. Small. 2023;19(9):2206258.
[19] Feng JH, Yang F, Qian SZ. Improving the bond between polypropylene fiber and cement matrix by nano calcium carbonate modification. Constr Build Mater. 2021;269:121249.
[20] Cui K, Lau D, Zhang Y, Chang J. Mechanical properties and mechanism of nano-$CaCO_3$ enhanced sulphoaluminate cement-based reactive powder concrete. Constr Build Mater. 2021;309:125099.
[21] Yang HS, Che YJ, Shi MY. Influences of calcium carbonate nanoparticles on the workability and strength of 3D printing cementitious materials containing limestone powder. J Build Eng. 2021;44:102976.
[22] Nejad F, Tolouei M, Nazari H, Naderan A. Effects of calcium carbonate nanoparticles and fly ash on mechanical and permeability properties of concrete. Adv Civ Eng Mater. 2018;7:651–68.
[23] Hakamy A. Effect of $CaCO_3$ nanoparticles on the microstructure and fracture toughness of ceramic nanocomposites. J Taibah Univ Sci. 2020;14:1201–7.
[24] Hodhod A, Zaki SI. Comparison between the effect of addition of nano-calcium carbonate and nano-kaoline on developing the properties of reinforced concrete. 10th International Conference on Nano-Technology in Construction. Vol. 3. 2018. p. 147–59.
[25] Sato T, Beaudoin JJ. The effect of nano-sized $CaCO_3$ addition on the hydration of OPC containing high volumes of ground granulated blast-furnace slag. In The 2nd International Symposium Advanced Concrete Science Engineering. Quebec City, Canada; 2006.
[26] JGJ63-2006. Standard of water for concrete. Beijing, China: Ministry of Construction of the People's Republic of China; 2006.
[27] GB/T 50080-2016. Standard for test method of performance on ordinary fresh concrete. Beijing, China: Ministry of Housing and Urban-Rural Development of the People's Republic of China; 2016.
[28] GB/T 1346-2011. Test Methods for Water Requirement of Normal Consistency, Setting Time and Soundness of the Portland Cement. Beijing, China: Standardization Administration of the People's Republic of China; 2011.
[29] Dong SF, Dong XF, Ashour A, Han BG, Ou JP. Fracture and self-sensing characteristics of super-fine stainless wire reinforced reactive powder concrete. Cem Concr Compos. 2020;105:103427.
[30] Han BG, Dong SF, Ou JP, Zhang CY, Wang YL, Xun Y, et al. Microstructure related mechanical behaviors of short-cut super-fine stainless wire reinforced reactive powder concrete. Mater Des. 2016;96(4):16–26.
[31] Hussin A, Poole C. Petrography evidence of the interfacial transition zone (ITZ) in the normal strength concrete containing granitic and limestone aggregates. Constr Build Mater. 2011;25:2298–303.
[32] Yu R, Spiesz P, Brouwers H. Effect of nano-silica on the hydration and microstructure development of ultra-high performance concrete (UHPC) with a low binder amount. Constr Build Mater. 2014;65:140–50.
[33] Pane I, Hansen W. Investigation of blended cement hydration by isothermal calorimetry and thermal analysis. Cem Concr Res. 2005;35(6):1155–64.
[34] Esping O. Effect of limestone filler BET (H_2O)-area on the fresh and hardened properties of self-compacting concrete. Cem Concr Res. 2008;38(7):938–44.
[35] Camiletti J, Soliman AM, Nehdi ML. Effects of nano- and micro-limestone addition on early-age properties of ultra high-performance concrete. Mater Struct. 2013;46(6):881–98.
[36] Lian HH, Sun XJ, Yu ZP, Yang T, Zhang JT, Li GC, et al. Research on the fracture mechanical performance of basalt fiber nano-$CaCO_3$ concrete based on DIC technology. Constr Build Mater. 2022;329:127193.
[37] Wang XY, Dong SF, Li ZM, Han BG, Ou JP. Nanomechanical characteristics of interfacial transition zone in nano-engineered concrete. Engineering. 2021;17:99–109.
[38] Tao M, Qian KL, Qian X, Zhan SL. Effect of the nano-$CaCO_3$ on hydrated properties and interface of cement paste. Rare Met Mat Eng. 2008;37:667–9.
[39] Luo XB, Si YY, Gu WQ. Effect of silica fume on mechanical properties of concrete incorporating steel slag powder. Wuhan Univ J Nat Sci. 2019;24:86–92.
[40] Vanitha N, Revathi T, Gopalakrishnan R, Jeyalakshmi R. Effect of TiO_2, Al_2O_3 and $CaCO_3$ nano-additives in singular, binary and

ternary forms on the mechanical, thermal and microstructural propertites of fly ash supplemented cement matrix. Mater Today: Proc. 2021;47:871–9.

[41] Yue YC, Zhou YW, Xing F, Gong GQ, Hu B, Guo MH. An industrial applicable method to improve the properties of recycled aggregate concrete by incorporating nano-silica and micro-$CaCO_3$. J Clean Prod. 2020;259:120920.

[42] Han BG, Zhang LQ, Zeng SZ, Dong SF, Yu X, Yang RW, et al. Nano-core effect in nano-engineered cementitious composites. Compos Part A: Appl Sci Manuf. 2017;95:100–9.

[43] Zhao YS, Gao JM, Liu CB, Chen XM, Xu ZH. The particle-size effect of waste clay brick powder on its pozzolanic activity and properties of blended cement. J Clean Prod. 2020;242:118521.

[44] Wu M, Zhang YS, Ji YS, Liu GJ, Liu C, She W, et al. Reducing environmental impacts and carbon emissions: Study of effects of superfine cement particles on blended cement containing high volume mineral admixtures. J Clean Prod. 2018;196:358–69.

[45] Batuecas E, Liendo F, Tommasi T, Bensaid S, Deorsola FA, Fino D. Recycling CO_2 from flue gas for $CaCO_3$ nanoparticles production as cement filler: A life cycle assessment. J CO_2 Util. 2021;45:101446.